RSC Advances

PAPER

View Article Online
View Journal | View Issue

Cite this: *RSC Adv.*, 2023, **13**, 9945

Towards quantum corrosion chemistry: screening perfect Cr, Ni sites and stoichiometry on top of an Fe(110) surface using DFT

Zhihao Yang,[a] Chi Zhang,[b] Shuo Wang,[a] Chengpeng Xue,[a] Guangyuan Tian,[a] Hui Su,[a] Chengming Yan,[a] Zhifei Yan,[c] Xiaoguang Liu[d] and Junsheng Wang *[ae]

For decades, corrosion has been classified into many categories according to the microstructural morphology of the chemical reaction products. Until recently, the development of quantum chemistry has simplified the fundamental corrosion mechanism into only two processes: electrochemical dissolution and hydrogen evolution reaction (HER). Although Cr and Ni elements have been found to segregate towards the surface of stainless steel to form a protective layer and prevent Fe dissolution, the understanding of the exact chemistry on top of the Fe surface has not been reported in previous studies. In this study, we have identified suitable doping sites for simultaneous doping of several Cr and Ni atoms, and quantified the effects of different alloy compositions ($Fe_{12}Cr_3Ni_1$, $Fe_{11}Cr_4Ni_1$, $Fe_{11}Cr_3Ni_2$, $Fe_{10}Cr_4Ni_2$, $Fe_{10}Cr_3Ni_3$) on the stability from two aspects: electron transfer and atomic dissolution. It was found that the doping atoms are more likely to be dispersed rather than aggregated in solid solution. When Cr atoms are symmetrically distributed and Ni atoms are located in the center, it is the site arrangement with the highest work function and stability. $Fe_{10}Cr_4Ni_2$ has been found to possess a higher electron binding capacity and thus higher electrode potentials. This is determined by the change of dipole caused by both electronegativity difference between atoms and polarization between the doped layer and the substrate layer. By calculating the vacancy formation energy, it is shown that $Fe_{11}Cr_4Ni_2$ is the perfect chemistry on top of the Fe(110) surface due to its high ability of preventing atomic dissolution.

Received 23rd November 2022
Accepted 14th March 2023

DOI: 10.1039/d2ra07463j

rsc.li/rsc-advances

1. Introduction

Iron-based alloys are widely used in modern industrial fields due to their abundant resources, low cost, good comprehensive performance, and wide range of performance.[1,2] However, on a global scale, corrosion has always been a key issue that causes technical and economic losses to industries, and may even bring risks and hazards to personal safety.[3,4] Therefore, the efforts on improving corrosion resistance have been a hot topic for the development of new iron-based alloys. By adding different kinds and proportions of alloying elements to iron, many new stainless steels have been created, which greatly improve the corrosion resistance of iron alloys. Ferrite is an α-Fe-based high alloyed steel with a Cr content of 15% to 30%. Good process ability and mechanical properties, excellent oxidation and corrosion resistance make ferrite widely used in proton exchange membrane fuel cells, automotive emission systems and many other fields.[5,6] The corrosion resistance of stainless steel is mainly attributable to the passive film, which protects the material from continuous corrosive attack by the external environment. However, the passivated surface usually has local defects, and active ions and ligands are easily adsorbed at these sites to cause local damage of the passivation film. Or under certain conditions, the passivation film may also be damaged or even removed by the impact of solid particles.[7] This leads to local metal exposure to corrosive media, resulting in localized corrosion, such as pitting corrosion, galvanic corrosion, *etc.*, which has a serious negative impact on the properties of the alloy.[8,9] Methods to resist this corrosion mainly include alloying element optimization and surface modification.[7] It is therefore necessary to understand the effect of alloying elements on the corrosion of clean surfaces without natural passive films to minimize the corrosion hazards of stainless steel.[10]

Researchers believe that Fe is easy to react with oxygen in humid environment and then corrosion occurs. The reaction formula is $4Fe + 3O_2 + 6H_2O = 4Fe(OH)_3$. Even at the high temperature of 600 °C, the presence of water vapor will still

[a]*School of Materials Science and Engineering, Beijing Institute of Technology, Beijing 100081, China. E-mail: junsheng.wang@bit.edu.cn; Tel: +86 10 68915043*
[b]*School of Materials Science and Engineering, Shenyang University of Technology, Shenyang 110870, China*
[c]*China North Industries Group, No. 52 Research Institute, Baotou, Inner Mongolia, 014030, China*
[d]*School of Materials Science and Engineering, University of Science & Technology Beijing, No. 30 Xueyuan Road, Beijing, 100083, China*
[e]*Advanced Research Institute of Multidisciplinary Science, Beijing Institute of Technology, Beijing 100081, China*

accelerate the corrosion.[11] For Fe used in seawater equipment, such as ships and naval vessels, since seawater is an electrolyte solution, it will undergo electrochemical corrosion, and the corrosion mechanism can be explained by the depolarization process of oxygen.[12] The rate of corrosion is directly related to the rate of oxygen diffusion in seawater. In addition, there are plenty of chloride ions in seawater, which will crack the oxide film on the metal surface, leading to stress corrosion cracking and pitting corrosion, and eventually the material properties degrade.[12,13] By experimenting on different alloying additions, many studies have improved significantly the corrosion resistance of ferroalloys, inventing various types of stainless steels with good corrosion resistance. Wang *et al.*[11] found that for Fe–Cr alloys in air, the oxidation rate decreases with the increase of Cr content. However, if the Cr content is increased to 15 wt% or higher, the mass of the alloy changes little due to the formation of protective Cr_2O_3 oxide film. Dong *et al.*[14] found that by adding 0.3 wt% Cu and 0.3 wt% Cr to the steel bar, the corrosion resistance of the steel bar has been increased by 46.3% compared with adding 0.2 wt% Ni and 0.15 wt% Mo, and Cr is one of the main elements to improve the protection of the corrosion layer of the steel bar. Tian *et al.*[15] believed that the surface oxide film of nickel-containing steel had a strong inhibition effect on corrosion attack. It can be found that the corrosion of ferroalloys by experimental methods is mostly concentrated on the passivation film and the corrosion layer, but it is difficult to study the corrosion resistance of the matrix itself.

Integrated Computational Materials Engineering (ICME) is a modern systems-based approach to designing materials that meet specific performance criteria by combining computational material models across multiple length scales.[16,17] Many properties of alloys can be readily predicted based on tools such as density functional theory (DFT).[18,19] It is generally believed that doping of alloying elements can change the atomic structure and electronic state of materials, thereby altering the physical and chemical properties of materials. The first-principles calculations based on DFT can analyze the corrosion mechanism from the perspective of the atomic scale, and obtain accurate results, which are difficult to achieve by traditional experimental techniques.[20,21] The first-principles calculation of work function reflect the electrode potential on the surface of the material, which can be used to evaluate the corrosion behavior of the materials.[22,23] Li *et al.*[24] obtained the intrinsic potential difference between each phase by calculating the work function of α-Fe (110) plane, martensite (110) and $(Fe,Cr)_{23}C_6$ (111), and then evaluated the effect of annealing treatment on the corrosion resistance of X_2CrNi_{12} steel by comparing the potential difference of each phase. Yin *et al.*[13] calculated the surface energy and work function of the Fe(110), Cr(110) and Fe(110) surface doped with Cr to study the surface properties of the alloy, and found that the surface energy increases while the work function does not change much after doping with one or two Cr. However, the work function decreased significantly after adding the solvation model. Many works also often use first-principles calculations to study the adsorption, dissociation and other interactions between small molecules and metal surfaces, and then to analyze the corrosion mechanism of metals. Hu *et al.*[25] studied the adsorption behavior of typical adsorbates H_2O, H^+, OH^-, Cl^- before and after doping Cr on Fe(110) surface based on DFT, and found that the Cr-doped Fe(110) surface is more stable than Fe(110) and Cr(110) surfaces. Cr doping greatly improves the electron-donating ability of adjacent Fe atoms, which in turn promotes the adsorption of positively charged H^+.

However, most of the above studies focus on the effect of single atom or atoms of the same species on the surface alloying of Fe, and few studies have been done on the effects of multiple atoms of different species doping simultaneous. Actually, the properties of stainless steel are often related to the interaction and common influence of various elements. In the work reported in this paper, we focus on the corrosion-related properties of Fe–Cr–Ni base stainless steel systems under different alloy compositions. The formation enthalpy, work function, and vacancy formation energy were calculated by first-principles calculations. We identified suitable doping sites for Cr and Ni and discussed the effects of doping concentration on Fe surface stability. This computational approach can be successfully used to explain experimental phenomena, predict properties and even design materials.[10] We hope that this study will help to reveal the mechanism of the effect of alloying elements on the corrosion of stainless steel at the atomic scale and provide a method that enables the rapid and large-scale search for new corrosion-resistant alloy systems, which is difficult for experimental research to achieve due to high cost and long period of time.

2. Computation methods

2.1 Models

All the simulation calculations in this study are conducted using spin-polarized density functional theory (DFT) as implemented in the Vienna *ab initio* simulation package (VASP).[26,27] The projector augmented wave (PAW) method is used to characterize the interactions of core and valence electrons.[28] The exchange–correlation effects are described using the Perdew–Burke–Ernzerhof (PBE) functions within the generalized gradient approximation (GGA).[29] In the process of structure optimization for bulk metallic Fe of bcc cell, the plane wave kinetic energy cutoff is 450 eV, and the Γ-centered *k*-point mesh is 17 × 17 × 17. The optimized lattice constant of Fe is 2.83 Å, which is in good agreement with the experimental value (a_1 = 2.86 Å)[30] as well as the previous DFT calculated values (a_2 = 2.841 Å and a_3 = 2.834 Å).[13,31]

Studies have shown that the (110) surface is the most stable surface and have the lowest energy among several low-index surfaces of bcc metals.[32,33] Therefore, in this study, Cr and Ni are doped on Fe(110) surface. The model contains 80 atoms, arranged in 5 atomic layers, with 16 atoms in each layer, as shown in Fig. 1. A 10 Å vacuum layer is set in the *c* direction to ensure that the vacuum layer is large enough to calculate the work function and other related data. The electrochemical stability and the corrosion behavior of metals are very sensitive to the surface properties, and anodic dissolution always

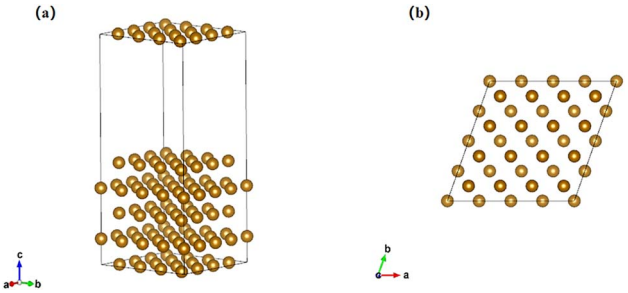

Fig. 1 The initial structure of Fe(110): (a) calculated slab model of Fe(110); (b) top view of the atomic structure of Fe(110).

happens at surfaces and charge transfer also takes place at the surface or interface.[34] Therefore, top surface layer doping is a reasonable and time-saving approach for studying the alloying effect on surface properties.[13] As a result, this study used the atomic replacement method to dope Cr and Ni with different sites and contents only in the first layer. During the optimization process, the two bottom layers are fixed at their bulk coordinates, and the three top Fe layers are relaxed, so that the model has a surface-block-like structure.[35] The Brillouin zone uses a $5 \times 5 \times 1$ k-point mesh for the Fe(110) surface.

2.2 Formation enthalpy

Formation enthalpy (ΔH) is an important physical parameter that can be used to assess the stability of a molecule and estimate the energy released in a reaction.[36] Formation enthalpy can be defined as the thermal effect of the most stable element in the standard state to generate the amount of a pure substance in the standard state at a certain temperature. Since the effect of pressure on the condensed phase is ignored in the calculation process, the energy calculated at 0 K does not have any entropy contribution, so the formation energy is exactly the formation enthalpy.[37]

The formation enthalpy of each atom in the Fe bulk after doping with Cr and Ni can be expressed by the following formula:[38,39]

$$\Delta H = \frac{E_{\text{total}} - NE_{\text{Fe}} - ME_{\text{Cr}} - XE_{\text{Ni}}}{N + M + X} \quad (1)$$

where E_{total} is the total energy of the relaxed Fe slab surface after doping with Cr and Ni, E_{Fe}, E_{Cr}, and E_{Ni} stand for the bulk energies of Fe, Cr, and Ni, N, M, and X refer to the number of Fe, Cr and Ni atoms in the slab respectively.

2.3 Work function

Work function (Φ) is the minimum energy required for electrons to transfer from the Fermi level to the vacuum level on the metal surface, reflecting the ability of electrons to escape from the surface of the material and become free electrons.[23,40] The work function is usually related to the distribution of electrons on the surface of the materials. The distribution of electrons on the surface can be changed by alloying, which in turn affects the physical and chemical properties such as bond strength and atomic stability.[41] The work function can be calculated by the following formula:[13,41]

$$\Phi = -e_{\varphi} - E_{\text{F}} \quad (2)$$

where $-e_{\varphi}$ is the electrostatic potential energy in vacuum, and E_{F} represents the Fermi level of the slab. A higher work function corresponds to a larger barrier for electrons to escape from the solid, and subsequent reactions requiring electrons are less easy to carry out and thus have better corrosion resistance.[34,41] From a thermodynamic point of view, the work function is closely related to the electrode potential and can be used to evaluate corrosion behavior. Materials with higher work function generally have higher corrosion potentials,[22,23] and corrosion reactions are more difficult to occur.

2.4 Vacancy formation energy

Vacancy formation energy (E_{vac}) refers to the energy required for atoms to break free from a material. The dissolution of atoms on the metal surface reflects the corrosion behavior of the metal to a certain extent. Therefore, we calculate the energy required for the dissolution of iron atoms to form vacancies by establishing a model for removing certain Fe atoms from the doped Fe surface. The vacancy formation energy can be calculated by the following formula:[42,43]

$$E_{\text{vac}} = E_{\text{slab+vac}} - E_{\text{slab}} + E_{\text{atom}} \quad (3)$$

where $E_{\text{slab+vac}}$ is the total energy of the slab model with one defect, E_{slab} is the energy of the complete slab model with no vacancy, and E_{atom} is the energy per atom for the bulk. Lower vacancy formation energy means that atoms need less energy to escape the surface and surface dissolution is more likely to occur.

3. Results and discussions

3.1 Selection of Cr and Ni doping sites on Fe surface

For most stainless steels, Cr and Ni elements account for the highest proportions besides Fe. Cr is the key alloying element to improve the corrosion resistance of stainless steel, due to its ability to inhibit water adsorption and increase surface electrode potential,[10] while Ni has a higher corrosion potential than Cr, and can also promote the phase balance, element partitioning and corrosion resistance in acids.[40] Therefore, this work attempts to study the corrosion behavior of the Fe–Cr–Ni basic system without considering the influence of Mn, Mo, Cu, Si, C and other trace elements or impurity elements.

To determine the content of Cr and Ni doped in Fe, we have analyzed the compositions of the common 316L stainless steel and the QN1906 and QN2109 stainless steels of Qingshan Group with good corrosion resistance. The atomic fractions of the three grades after simplification are $Fe_{11.64}Cr_{2.84}Ni_{1.51}$, $Fe_{11.6-12.2}Cr_{3.1-3.4}Ni_{0.7-1.1}$, $Fe_{10.8-11.4}Cr_{3.4-3.7}Ni_{1.2-1.5}$. Five different stainless steel compositions can be approximated after integration, namely $Fe_{12}Cr_3Ni_1$, $Fe_{11}Cr_4Ni_1$, $Fe_{11}Cr_3Ni_2$, $Fe_{10}Cr_4Ni_2$, $Fe_{10}Cr_3Ni_3$. Therefore, in the first layer of Fe (110)

surface, 16 atoms were replaced according to the above five compositions. However, since there are many arrangement options for the replacement sites in the 16 atoms, we first need to determine which arrangement Cr and Ni are more likely to be solvable. Therefore, the main content of this section is to find the most suitable doping sites for Cr and Ni on the surface of Fe (110) by calculating the formation enthalpy and work function.

We modeled various site schemes for the chemical compositions of $Fe_{12}Cr_3Ni_1$ and $Fe_{11}Cr_4Ni_1$ first and then calculated their formation enthalpies which are shown in Fig. 2 and 3. For the sake of clarity, only the top view of the arrangement of atoms in the first layer is shown. The model can be roughly divided into symmetric distribution of dopant atoms (A1, A2, B1, B2), distribution of dopant atoms with the farthest distance (A3, B3, B4), aggregated distribution of dopant atoms (A4, B5, B6), linear distribution of dopant atoms (A5).

The level of formation enthalpy directly reflects the difficulty of solid solution formation. As shown in Fig. 2 and 3, we found that the formation enthalpies when the dopant atoms are aggregated or in a straight line (A4, A5, B5, B6) are generally 0.01–0.02 eV per atom higher than the formation enthalpies when the dopant atoms are dispersed (A1, A2, A3, B1, B2, B3, B4). This shows that the Fe(110) surface where the dopant atoms are aggregated is unstable, and Cr and Ni tend to be dissolved in a dispersed form. This is because the electronegativity of Cr is lower than that of Fe and Ni, so Cr doping on the Fe surface is more inclined to release electrons. When multiple Cr atoms aggregate, the electrons released by Cr will be unevenly distributed on the Fe surface, which will change the surface electron density distribution and improve the surface activity.

To further determine the substitution sites of the dopant atoms, we calculated the work functions of $Fe_{12}Cr_3Ni_1$ and

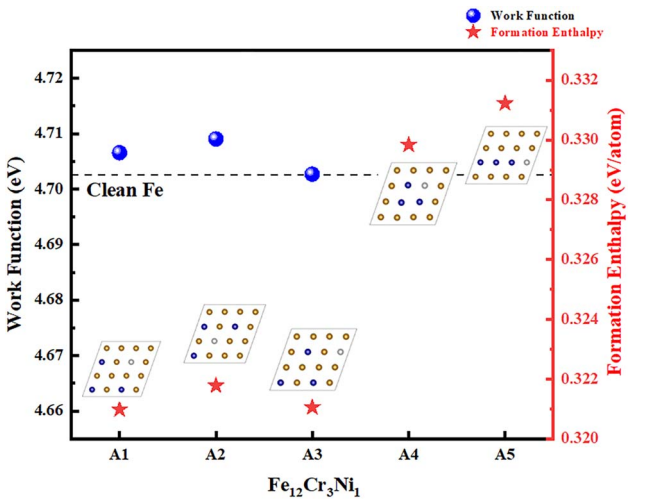

Fig. 2 The work functions and the formation enthalpies of Fe(110) surface doped with three Cr atoms and one Ni atom. The illustrations show the corresponding atomic structures of the first layer of Fe(110) surface. The yellow atoms, blue atoms and white atoms represent Fe, Cr and Ni, respectively. The dashed line indicates the work function of the clean Fe surface.

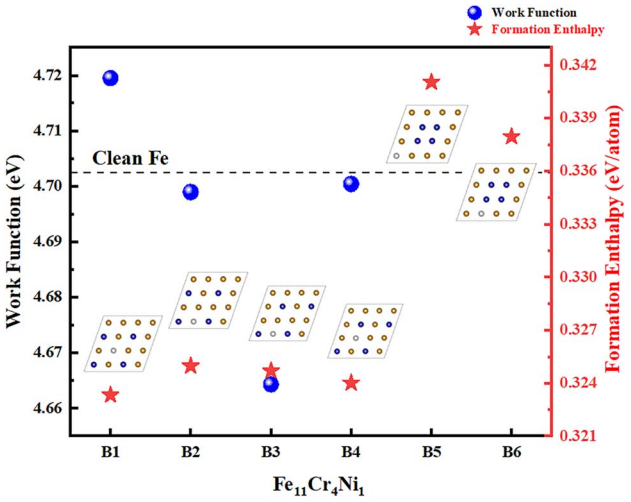

Fig. 3 The work functions and the formation enthalpies of Fe(110) surface doped with four Cr atoms and one Ni atom. The illustrations show the corresponding atomic structures of the first layer of Fe(110) surface.

$Fe_{11}Cr_4Ni_1$ when the atoms are dispersed (A1, A2, A3, B1, B2, B3, B4), as shown in Fig. 2 and 3. The work function can well reflect the overall ability of the surface to bind electrons. The surface with a lower work function has a weaker ability to bind electrons, and the electrons are usually more easily transferred, which in turn affects the occurrence of surface chemical reactions.[41,44] The calculated work function value of clean Fe(110) surface is 4.702 eV, which is consistent with 4.74 eV and 4.79 eV in the previous studies.[13,33] We found that A2 and B1 were the two structures with the highest work functions, both of which have a symmetrical distribution of Cr as Ni atoms are at the center of Cr atoms, indicating that the ferroalloys with this arrangement is less prone to lose electrons.

Furthermore, to determine the site arrangement when Ni is increased by one more than before, we continued to calculate the formation enthalpy and work function of several different models of $Fe_{10}Cr_4Ni_2$. According to the above findings, four Cr atoms were fixed on the evenly distributed sites, and Ni atoms take a random distribution, as shown in Fig. 4. It can be found that the formation enthalpy is in good agreement with the work function, and the formation enthalpy of the structure with higher work function is correspondingly lower. This is because they are all affected by the electron density distribution on the solid surface,[45] and a surface with a higher work function will have a higher electron binding capacity and a lower surface activity, resulting in a lower formation enthalpy and a more stable structure. It can be seen that the work functions of structures C3 and C4 are the highest. In fact, the Ni atoms after expanding these two structural units are exactly located at the central site of the Cr atoms, which is consistent with the previous conclusions on $Fe_{12}Cr_3Ni_1$ and $Fe_{11}Cr_4Ni_1$. This further demonstrates that Cr atoms are symmetrically distributed and Ni atoms are located in the center, which is the most stable site arrangement with the highest work function. In fact, the electronegativity of solid solution atoms can affect the

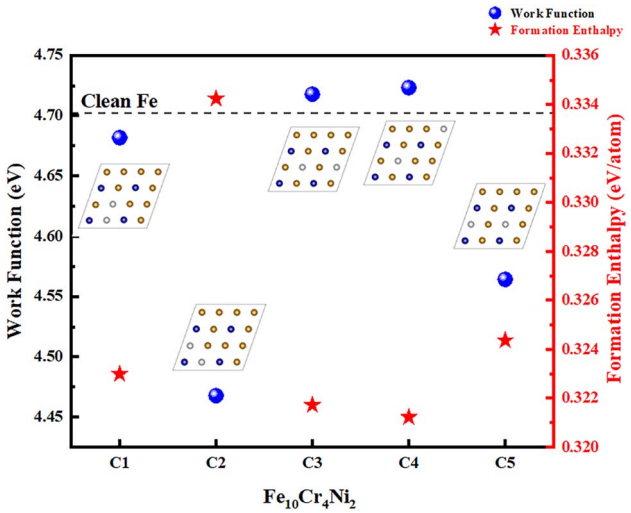

Fig. 4 The work functions and the formation enthalpies of Fe(110) surface doped with four Cr atoms and two Ni atoms. The illustrations show the corresponding atomic structures of the first layer of Fe(110) surface.

number and direction of surface electron transfer, resulting in changes in the distribution of surface electrons, which in turn alters the work function.[34] When the electronegativity of the dopant atoms is higher than that of the base atoms, the adjacent base atoms will transfer electrons to the dopant atoms and make the dopant atoms negatively charged, which will lead to a negative electric dipole moment on the metal surface, thereby increasing the work function.[41,46] The relative electronegativities of Cr, Fe and Ni are 1.66, 1.83 and 1.91, respectively. It can be found that the difference in electronegativity between Cr and Ni is larger than that of Cr and Fe. When Ni is located in the center, the surrounding atoms, especially Cr, will transfer a large number of electrons to Ni, which thus produces a relatively negative electric dipole moment, resulting in a larger work function. It is worth mentioning that when we calculated the $Fe_{10}Cr_4Ni_2$ composition, we also tried the structure of doped atoms with aggregated distribution, and found that it is difficult to relax, indicating that this is an unstable structure. This is consistent with the conclusions drawn above in terms of $Fe_{12}Cr_3Ni_1$ and $Fe_{11}Cr_4Ni_1$ compositions.

3.2 Stability of the Fe surface with different doping compositions

The addition of alloying elements can significantly change the physical and chemical properties of the Fe surface. Different alloying elements would result in the changes of atomic structure and electron distributions on the surface, which would in turn vary the thermodynamic stability of the Fe surface. This effect on the stability changes the energy required for the electron transfer of the Fe surface and the separation of atoms from the Fe surface, both of which are closely related to the anodic dissolution behavior of Fe alloys, reflecting the corrosion resistance of ferroalloys to some extent.

3.2.1 Work function. As mentioned above, the work function is a fundamental electronic parameter that represents the minimum energy required for electrons to escape from the metal surface and is closely related to the electrode potential of the metal.[23,24] Doping atoms cause electron rearrangement on the metal surface and play an important role in the electronic behavior, which in part determines the electrochemical activity or reactivity.[23,44] Higher work function corresponds to stronger overall electron confinement, resulting in stronger atomic bonding and stability, with the potential for better corrosion resistance.[47,48]

In Section 3.2, we have found the most suitable doping sites for Cr and Ni, and calculated the highest work function under the three chemical compositions including $Fe_{12}Cr_3Ni_1$, $Fe_{11}Cr_4Ni_1$ and $Fe_{10}Cr_4Ni_2$. In this section, the work functions of $Fe_{11}Cr_3Ni_2$ and $Fe_{10}Cr_3Ni_3$ are presented, as shown in Fig. 5. The illustrations show the possible doping types with $Fe_{11}Cr_3Ni_2$ composition and $Fe_{10}Cr_3Ni_3$ composition in which Cr atoms are symmetrically distributed and Ni atoms are located in the center. For $Fe_{11}Cr_3Ni_2$, it can be seen that the work functions of the three are higher than that of the clean Fe surface and the D3 arrangement has the highest work function. In addition, we also calculated their formation enthalpies, and found only a 10^{-4} order of magnitude difference, which shows the reliability of the conclusion in Section 3.1. Similarly, for $Fe_{10}Cr_3Ni_3$, it can be seen that the work function is not much different, and the difference in their formation enthalpies has reached the order of 10^{-5} which is negligible.

In order to compare different compositions, we have listed the highest work functions of them in a graph, as shown in Fig. 6. It can be found that $Fe_{10}Cr_4Ni_2$ composition has the highest work function, followed by the work function of $Fe_{11}Cr_4Ni_1$. When the Cr content increases, the work function of the Fe alloy increases significantly; when the Cr content remains unchanged, a moderate increase in the Ni content also

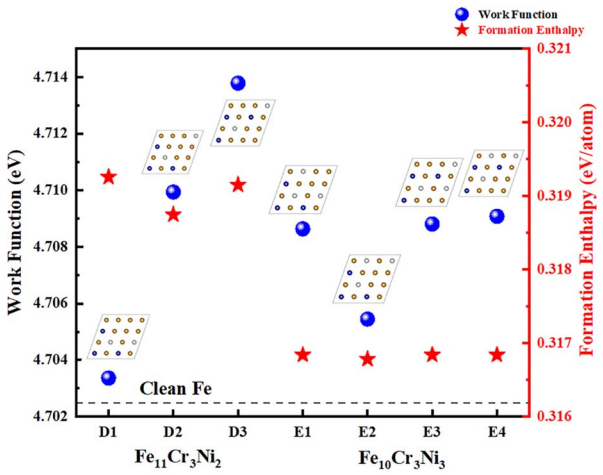

Fig. 5 The work functions and the formation enthalpies of Fe(110) surface doped with three Cr atoms and two Ni atoms (D1, D2, D3), four Cr atoms and two Ni atoms (E1, E2, E3, E4). The illustrations show the corresponding atomic structures of the first layer of Fe(110) surface.

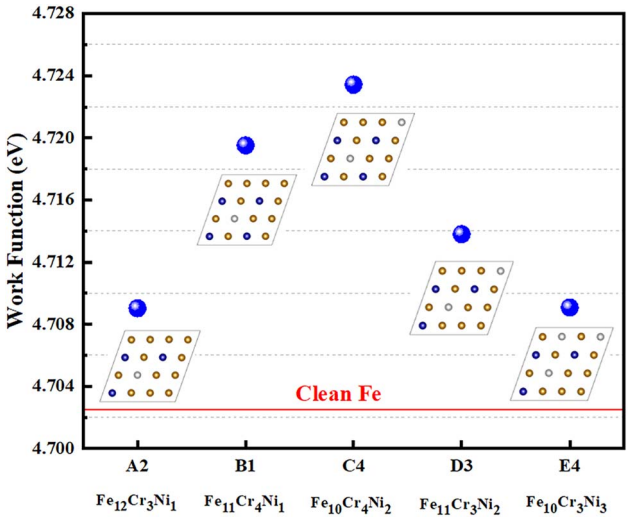

Fig. 6 The work functions of Fe(110) surface with five compositions. The illustrations show the corresponding atomic structures of the first layer of Fe(110) surface. The red line indicates the work function of the clean Fe surface.

increases the work function of the Fe alloy. However, when the Ni content increases to the same level as Cr ($Fe_{10}Cr_3Ni_3$), the contribution of Ni to the work function is not obvious or even tends to decrease. As we mentioned above, the effect of dopant atoms on the work function of the metal surface depends on the electronegativity of the dopant atoms.[34] It is generally believed that if the electronegativity of the dopant atoms is greater than that of the substrate atoms, electrons will not only be transferred to the dopant atoms in the surface layer, but also transferred from the substrate layer to the dopant layer, resulting in excessive negative charges in the surface layer and excessive positive charges below the surface layer. This will create a negative dipole moment that points inwards, strengthening the dipoles of the original surface and increasing the work function.[41,49] However, the electronegativity of Cr is lower than that of Fe and Ni, while Ni has the highest electronegativity. It seems that the results do not fit the traditional interpretation between work function change and charge transfer. The reasons why the simple electronegativity argument fails have been discussed previously.[46,50] In fact, the change in work function depends not only on pure charge transfer, but also on the details of charge redistribution. For Fe–Cr–Ni alloys, there are basically metallic bonds, and the change in charge density is complicated, which has been explained with the general method proposed by Leung *et al.*[46,50] They reported that the changes in work function were related to changes in dipole from both charge transfer and polarization. The theory explains the relationship among work function change, charge transfer, and polarization, which can be described by the following formula:[46,49]

$$\Delta\Phi = -\frac{e}{\varepsilon_0}[\Delta P_1 + \Delta P_2 + (P_s - P_0)] \quad (4)$$

where $\Delta\Phi$ is the work function change, e is the fundamental charge, ε_0 is the dielectric constant in vacuum, ΔP_1 refers to the change in surface dipole density as a result of charge transfer due to the difference in electronegativity, and ΔP_2 represents the change in surface dipole density caused by the polarization between the doped layer and the substrate layer. P_s is the surface dipole density of the Fe substrate and P_0 is the surface dipole density of the clean Fe surface (fully relaxed). The change represented by $(P_s - P_0)$ term is due to the relaxation of the substrate induced by the overlayer. $(P_s - P_0)$ is usually much smaller than the ΔP_1 and ΔP_2 terms, and is taken as a secondary correction.

From above relationship, it is believed that the work function of a surface can be determined by the charge transfer caused by the difference in electronegativity of atoms, as given by ΔP_1. Besides, the polarization between the layers can also result in the change in work function, as given by ΔP_2. We believe that when the doping concentration of Cr reaches a certain level, the dipole change caused by the polarization between the doped layer and the substrate layer will play a dominant role. It will alter the sign of the dipole on the Fe surface, so the work function increases with increasing Cr content. When the Cr content remains unchanged, the charge transfer caused by an appropriate increase in Ni can generate a new negative dipole moment, thereby increasing the work function. However, when the amount of doping Ni atoms continues to increase, the polarization induced by Cr will be weakened, and the work function will tend to decrease. Therefore, the doping amount of Ni should be moderate. In previous reports by Sun *et al.*,[49] it was found that doping Cr on the surface of Ni metal has a similar behavior as doping Cr on Fe surfaces. When the content of Cr on the surface of Ni (111) and (100) reaches 4Cr and 6Cr, respectively, the surface work function will increase with the Cr doping amount, which is a result of the dipole change due to the polarization between the doped layer and the underlying substrate.

3.2.2 Vacancy formation energy. The anodic dissolution of Fe alloy surfaces mainly includes two processes, namely electron transfer and surface atomic dissolution. In Section 3.2.1 we mainly discussed the effect of alloying on the electron transfer ability. After the solid solution of alloying elements on the Fe(110) surface, it can alter the surface atomic structure and charge distribution state, so that the energy required for Fe to escape from the surface and dissolve will change, which is the change of the vacancy formation energy. Therefore, discussing the vacancy formation energy under different doping schemes is of great significance to study the anodic dissolution process and the stability of alloys. In this section, we will continue to study the vacancy formation energies at two chemistries of $Fe_{11}Cr_4Ni_1$ and $Fe_{10}Cr_4Ni_2$ with higher work functions.

Since there are several Fe atoms on the surface, Fe atoms at different sites will have different changes in atomic structure such as spatial displacement, and the bond length and bond strength formed with surrounding atoms will also be different. Therefore, the vacancy formation energy of Fe atoms at different sites will be bound to be different. In order to produce comprehensive and objective analysis, we differentiated Fe

atoms at different sites with Ni as the center according to the principle of equivalence, namely the first, second nearest neighbor of doped atoms, and so on, as shown in Fig. 7(a). For the $Fe_{11}Cr_4Ni_1$ composition, there are four difference sites: 1st nearest neighbor (yellow atoms), 2nd nearest neighbor (red atoms), 3rd nearest neighbor (green atoms) and 4th nearest neighbor (purple atoms). However, $Fe_{10}Cr_4Ni_2$ only has Fe atoms at two different sites: 1st nearest neighbor (yellow atoms) and 2nd nearest neighbor (red atoms).

In Fig. 7(b), we calculated the vacancy formation energies of the first, second, third and fourth nearest neighbor Fe atoms of doped atoms on the Fe(110) surface with two compositions. The vacancy formation energy is the energy required for atoms to escape from the metal surface, so the higher the vacancy formation energy, the more stable the iron atom at the site is. Conversely, the lower it is, the easier it is for atoms to escape from the surface, and the surface dissolution is more likely to occur.[41] By comparing the vacancy formation energies at different sites, we can see that the second nearest neighbors of doped atoms require higher energy to escape the surface under both compositions, and the first nearest neighbor is the lowest. For $Fe_{11}Cr_4Ni_1$ composition, the Fe atomic vacancy formation energy of the third and fourth neighbors is between the first and second neighbors. This is because the doping of Cr and Ni will change the distance between the first neighbor Fe atom and the doped atom, and in turn change the distance between the first neighbor and the second neighbor atom. This change has an important effect on the local atomic structure, thus changing the surface vacancy formation energy. More importantly, the vacancy formation energy of the first and second nearest neighbor Fe atoms of the chemistry $Fe_{10}Cr_4Ni_2$ is higher than that of $Fe_{11}Cr_4Ni_1$, which indicates that when 4 Cr atoms are doped, the addition of two Ni atoms is more conducive to the stability of Fe atoms. Combined with the conclusions in 3.2.1,

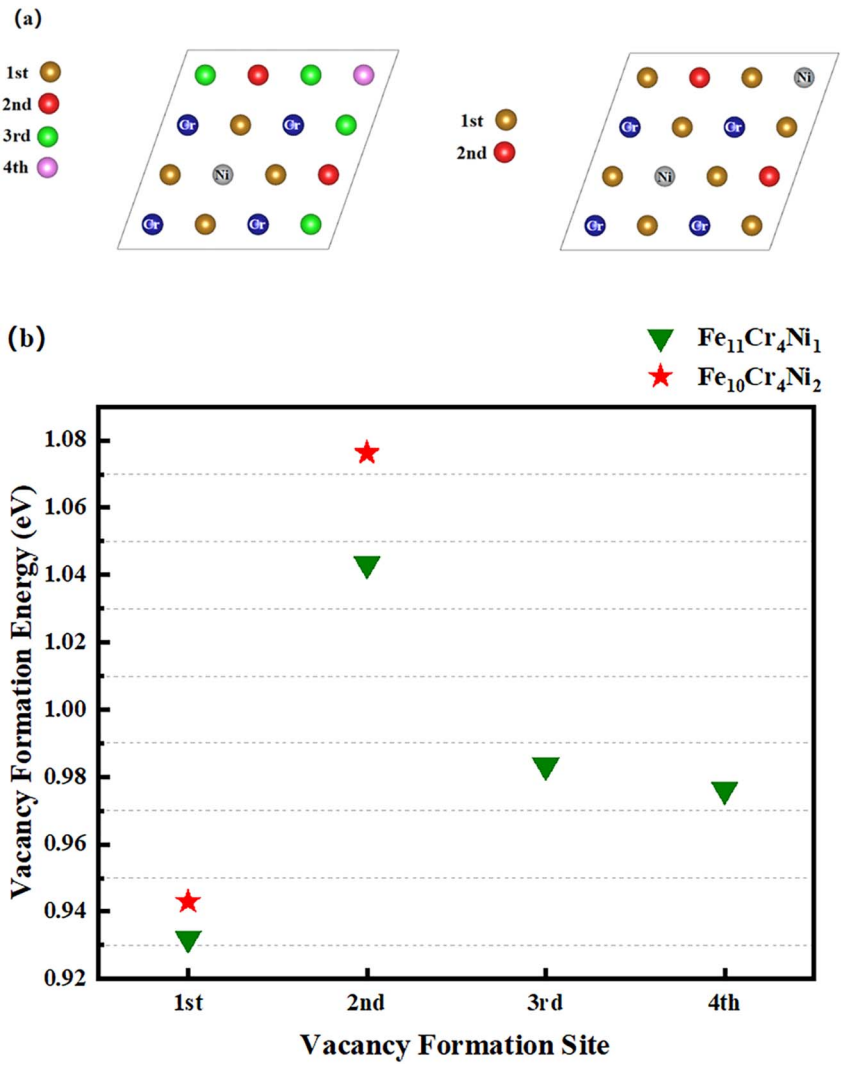

Fig. 7 (a)Vacancy formation energies of Fe atoms on Fe(110) surface doped with four Cr atoms and one Ni atom ($Fe_{11}Cr_4Ni_1$, left), four Cr atoms and two Ni atoms ($Fe_{10}Cr_4Ni_2$, right). The yellow atoms, red atoms, green atoms and purple atoms represent the first, second, third and fourth nearest neighboring Fe atom of the dopant, respectively; (b) vacancy formation energies of the first, second, third and fourth neighbors of doped atoms on Fe(110) surface with two compositions.

$Fe_{10}Cr_4Ni_2$ not only has a strong electron binding ability, but also has the potential to improve the stability of the first and second nearest neighbor Fe atoms, which reduces the anodic dissolution process of Fe to a certain level. However, it should be pointed out that the third nearest neighbor Fe atoms of $Fe_{11}Cr_4Ni_1$ (the green atoms in Fig. 7(a)) becomes the first nearest neighbor Fe atoms of $Fe_{10}Cr_4Ni_2$ when one more Ni is doped. For those four atoms in the model, the vacancy formation energy is reduced and there is a possibility of easier dissolution.

4. Conclusions

Based on first-principles calculations, the appropriate doping sites of alloying elements Cr and Ni on the Fe(110) surface were analyzed, and the effects of different alloy compositions ($Fe_{12}Cr_3Ni_1$, $Fe_{11}Cr_4Ni_1$, $Fe_{11}Cr_3Ni_2$, $Fe_{10}Cr_4Ni_2$, $Fe_{10}Cr_3Ni_3$) on the surface stability of Fe(110) surface were also studied. We calculated the work function of Fe(110) surface and the vacancy formation energy of each Fe atomic site under different doping amounts, and studied the anodic dissolution process from the two aspects of electron transfer and atomic dissolution, which are then used as an indicator of the corrosion resistance of Fe alloys. The main conclusions are as follows:

(1) By comparing the formation enthalpies and work functions of various doping schemes of $Fe_{12}Cr_3Ni_1$, $Fe_{11}Cr_4Ni_1$ and $Fe_{10}Cr_4Ni_2$, it is found that the doping atoms are more likely to be dispersed rather than aggregated in solid solution. When the Cr atoms are symmetrically distributed and the Ni atoms are located in the center, the structure has the highest work function and the most stable site arrangement.

(2) Doping atoms have a great influence on the electron transfer on the Fe surface, and the work functions of the five calculated chemistries are ranked as follows: $Fe_{10}Cr_4Ni_2$ > $Fe_{11}Cr_4Ni_1$ > $Fe_{11}Cr_3Ni_2$ > $Fe_{10}Cr_3Ni_3$ > $Fe_{12}Cr_3Ni_1$. This shows that $Fe_{10}Cr_4Ni_2$ has the strongest electron binding ability among the five concentrations with the possibility of the highest corrosion potential. The increase of Cr content led to the increase of the work function of Fe(110) surface, while the addition of Ni is moderate, the excess of which on the surface will result in the decrease of the work function.

(3) By calculating the vacancy formation energies under $Fe_{10}Cr_4Ni_2$ and $Fe_{11}Cr_4Ni_1$ chemical compositions, it is found that the first neighbor of the dopant atoms is more unstable than the second neighbor, and the third and fourth neighbors of $Fe_{11}Cr_4Ni_1$ are in between. $Fe_{10}Cr_4Ni_2$ has higher vacancy formation energies of the first and second nearest neighbor Fe atoms than $Fe_{11}Cr_4Ni_1$, indicating that most Fe atoms are more stable under the former composition, so it is more difficult to dissolve for surface atoms. However, since the first-neighbor sites under the two compositions are not exactly one-to-one correspondence, a small number of atoms in the model of $Fe_{10}Cr_4Ni_2$ may be more likely to escape than $Fe_{11}Cr_4Ni_1$.

Furthermore, this study provides a simple and efficient method of first-principles calculations for screening doping schemes and predict the corrosion resistance of alloying additions.

Conflicts of interest

The authors declare that they have no known competing financial interests or personal relationships that could have appeared to influence the work reported in this paper.

Acknowledgements

The authors appreciate tremendous helps from all members at the Integrated Computational Materials Engineering (ICME) lab, Beijing Institute of Technology, China. The research work is financially supported by National Natural Science Foundation of China (project number: 52073030) and National Natural Science Foundation of China-Guangxi Joint Fund (U20A20276).

References

1 Y. Zeng, M. Yu, Y. Meng, P. Fang, X. Lu and Y. Tong, *Adv. Energy Mater.*, 2016, **6**, 1601053.
2 L. Martinelli, F. Balbaud-Célérier, A. Terlain, S. Delpech, G. Santarini, J. Favergeon, G. Moulin, M. Tabarant and G. Picard, *Corrosion Sci.*, 2008, **50**, 2523–2536.
3 J. Potgieter, P. Olubambi, L. Cornish, C. Machio and E.-S. M. Sherif, *Corros. Sci.*, 2008, **50**, 2572–2579.
4 T. Duong, Y. Wang, X. Yan, A. Couet and S. Chaudhuri, *arXiv*, preprint, arXiv:2104.10590, 2021.
5 K. Cashell and N. Baddoo, *Thin-Walled Struct.*, 2014, **83**, 169–181.
6 Y. Inoue and M. Kikuchi, *Nippon Steel Technical Report No. 88*, July 2003.
7 T. Zhang and D. Li, *J. Mater. Sci.*, 2001, **36**, 3479–3486.
8 C. Punckt, M. Bolscher, H. H. Rotermund, A. S. Mikhailov, L. Organ, N. Budiansky, J. R. Scully and J. L. Hudson, *Science*, 2004, **305**, 1133–1136.
9 M.-F. Ng, D. J. Blackwood, H. Jin and T. L. Tan, *J. Phys. Chem. C*, 2020, **124**, 13799–13808.
10 C. Han, C. Zhang, X. Liu, H. Huang, S. Zhuang, P. Han and X. Wu, *J. Mol. Model.*, 2015, **21**, 1–9.
11 F. Wang and Y. Shu, *Oxid. Met.*, 2003, **59**, 201–214.
12 L. Yang, C. Bo, W. Junwei, W. Zhiping and L. Wensheng, *Rare Met. Mater. Eng.*, 2014, **43**, 17–23.
13 X. Yin, H. Wang, S. Sun and E.-H. Han, *Mater. Today Commun.*, 2020, **24**, 101122.
14 B. Dong, W. Liu, L. Chen, T. Zhang, Y. Fan, Y. Zhao, S. Li, W. Yang and W. Banthukul, *Cem. Concr. Compos.*, 2022, **125**, 104317.
15 Y. Tian, C. Dong, G. Wang, X. Cheng and X. Li, *Cem. Concr. Compos.*, 2020, **246**, 118462.
16 C. Kuehmann and G. Olson, *Mater. Sci. Technol.*, 2009, **25**, 472–478.
17 P. Lu, J. E. Saal, G. B. Olson, T. Li, O. J. Swanson, G. Frankel, A. Y. Gerard, K. F. Quiambao and J. R. Scully, *Scr. Mater.*, 2018, **153**, 19–22.
18 S. Wang, C. Zhang, X. Li, H. Huang and J. Wang, *J. Mater. Sci. Technol.*, 2020, **58**, 205–214.
19 S. Wang, J. Wang, C. Zhang and C. Xue, *J. Alloys Compd.*, 2022, **904**, 163800.

20 X. Li, C. Zhang, J. Wang, H. Huang and S. Wang, *Corros. Sci.*, 2020, **167**, 108549.
21 S. Bhasker-Ranganath, C. Wick and B. Ramachandran, *Mater. Today Chem.*, 2020, **17**, 100298.
22 J. Yao, N. Li, H. Grothe, Z. Qi and C. Dong, *Appl. Surf. Sci.*, 2021, **554**, 149597.
23 W. Li and D. Li, *Acta Mater.*, 2006, **54**, 445–452.
24 R. Li, B.-g. Fu, T.-s. Dong, G.-l. Li, J.-k. Li, X.-b. Zhao and J.-h. Liu, *J. Mater. Res. Technol.*, 2022, **18**, 448–460.
25 J. Hu, C. Wang, S. He, J. Zhu, L. Wei and S. Zheng, *Coatings*, 2018, **8**, 51.
26 G. Kresse and J. Hafner, *Phys. Rev. B: Condens. Matter Mater. Phys.*, 1993, **47**, 558.
27 G. Kresse and J. Furthmüller, *Phys. Rev. B: Condens. Matter Mater. Phys.*, 1996, **54**, 11169–11186.
28 P. Blöchl, O. Jepsen and O. Andersen, *Phys. Rev. B: Condens. Matter Mater. Phys.*, 1994, **50**, 17953–17979.
29 J. P. Perdew, K. Burke and M. Ernzerhof, *Phys. Rev. Lett.*, 1996, **77**, 3865.
30 C. Kittel, *Introduction to Solid State Physics* New York, 7th edn, 1976.
31 D. Jiang and E. A. Carter, *Surf. Sci.*, 2003, **547**, 85–98.
32 J. Wang and S.-Q. Wang, *Surf. Sci.*, 2014, **630**, 216–224.
33 R. Tran, X.-G. Li, J. H. Montoya, D. Winston, K. A. Persson and S. P. Ong, *Surf. Sci.*, 2019, **687**, 48–55.
34 Z. Luo, H. Zhu, T. Ying, D. Li and X. Zeng, *Surf. Sci.*, 2018, **672**, 68–74.
35 J. A. Yuwono, N. Birbilis, R. Liu, Q. Ou, Q. Bao and N. V. Medhekar, *J. Electrochem. Soc.*, 2017, **164**, C918.
36 S. J. Mole, X. Zhou and R. Liu, *J. Phys. Chem.*, 1996, **100**, 14665–14671.
37 H. Zhang, S. Shang, J. E. Saal, A. Saengdeejing, Y. Wang, L.-Q. Chen and Z.-K. Liu, *Intermetallics*, 2009, **17**, 878–885.
38 G. Ghosh and M. Asta, *Acta Mater.*, 2005, **53**, 3225–3252.
39 C. Wolverton, V. Ozoliņš and M. Asta, *Phys. Rev. B: Condens. Matter Mater. Phys.*, 2004, **69**, 144109.
40 B. Jiang, T. Guo, Q. Peng, Z. Jiao, A. A. Volinsky, L. Gao, Y. Ma and L. Qiao, *Corros. Sci.*, 2019, **157**, 498–507.
41 C. Zhang, J. Wang, X. Li, S. Wang, S. Zhu and S. Guan, *Phys. Chem. Chem. Phys.*, 2021, **23**, 26887–26901.
42 A. Sumer and S. Chaudhuri, *Corrosion*, 2017, **73**, 596–604.
43 H. Ma, X.-Q. Chen, R. Li, S. Wang, J. Dong and W. Ke, *Acta Mater.*, 2017, **130**, 137–146.
44 H. L. Skriver and N. Rosengaard, *Phys. Rev. B: Condens. Matter Mater. Phys.*, 1992, **46**, 7157.
45 E. Zuo, X. Dou, Y. Chen, W. Zhu, G. Jiang, A. Mao and J. Du, *Surf. Sci.*, 2021, **712**, 121880.
46 T.-C. Leung, C. Kao, W. Su, Y. Feng and C. T. Chan, *Phys. Rev. B: Condens. Matter Mater. Phys.*, 2003, **68**, 195408.
47 X. Huang, H. Lu and D. Li, *Mater. Chem. Phys.*, 2016, **173**, 238–245.
48 P. Bergveld, J. Hendrikse and W. Olthuis, *Meas. Sci. Technol.*, 1998, **9**, 1801.
49 X.-F. Sun, H.-T. Wang and E.-H. Han, *Acta Metall. Sin.*, 2019, **32**, 461–470.
50 G. Xu, Q. Wu, Z. Chen, Z. Huang and Y. P. Feng, *J. Appl. Phys.*, 2009, **106**, 043708.